Journal of Computational and Applied Mechanics, Vol. 8., No. 2., (2007), pp. 149–161

VORTEX CLOUD FLOW MODELLING OF CYLINDERS IN ORBITAL MOTION AT LOW REYNOLDS NUMBERS AND COMPARISONS WITH SOME PUBLISHED GRID-BASED CFD PREDICTIONS

R.Ivan Lewis
2-16 Bruce Building, Newcastle University
Newcastle upon Tyne, NE1 7RU, U.K.
r.i.lewis@ncl.ac.uk

[Received: January 11, 2007]

Abstract. Cylinders in elliptical orbital motion at low Reynolds numbers (Re) have been fairly extensively researched by grid-based Computational Fluid Dynamic (CFD) methods, revealing discontinuous behaviour of the root mean square (rms) lift coefficient from positive to negative values for low transverse amplitudes and orbital periodicity close to the Strouhal number for the fixed cylinder. Following published grid-based analyses, this paper studies a few flows for Re values of 130, 160 and 180 with orbital periodicity set at 85 % of the Strouhal frequency. The orbital amplitude in the mainstream flow direction Ax is fixed at 0.3 of the cylinder diameter, while the transverse amplitude is varied over the range $0 < A_y < 0.3$. A brief outline of the vortex cloud analysis is first given followed by a presentation of predicted lift and drag coefficients for this range of flow conditions plus selected flow patterns for regions of main interest. While the detailed predicted C_{Lmean} results are not identical to the published grid-based analysis, similar proneness to this switching phenomenon is found to occur. The flow mechanism underlying this is shown to be that of vortex pair formation in the downstream wake and is illustrated by predicted vortex-cloud patterns.

Keywords: vortex cloud modelling, cylinder wake flows, cylinder orbital motion

1. Introduction

Formation of vortex streets behind bluff bodies has fascinated large numbers of researchers since the early experiments of Strouhal [1] in 1878 concerning the generation of 'Aeolean tones' and the famous 1911 paper by Theodore von Kármán [2] bequeathing his name to the 'von Kármán vortex street'. Vortex streets are created as the outcome of periodic shedding of vorticity created initially at the surface and subsequently diffused and convected within the body boundary layer. The consequent fluctuations result in large periodic variation of the lift and drag forces and their associated lift and drag coefficients C_L and C_D defined as follows for a cylinder of

diameter d in a uniform stream U_∞

$$C_L = \frac{L}{\frac{1}{2}\rho U_\infty^2 d}, \quad C_D = \frac{D}{\frac{1}{2}\rho U_\infty^2 d}. \tag{1.1}$$

Shedding frequency f_v is categorised by the dimensionless Strouhal number S_t defined

$$S_t = \frac{f_v d}{U_\infty}. \tag{1.2}$$

As discussed elsewhere [3-5], the onset of regular vortex street shedding occurs above Re $\approx$ 47 and remains two-dimensional in character until Re $\approx$ 190, above which, as convective processes gain ascendency over viscous diffusion, three-dimensional instabilities begin to occur as proven theoretically by Barkley and Henderson [6] and Posdziech and Grundmann [7] and experimentally by Williamson [8]. The present studies using two-dimensional modelling are thus restricted to this range but towards the upper end for the three values Re = 130, 160 and 180 for which convective processes begin to dominate.

Because of vortex wake periodicity, flexibly mounted bodies such as struts, heat exchanger tubes, chimney stacks etc. may deflect and oscillate in response to these forces, possibly in linear or orbital motion. In such cases the vortex shedding properties will change resulting in quite different lift and drag variations with time. The main aim of this paper is to simulate these conditions for a cylinder in elliptical orbital motion at low Reynolds numbers. Studies of this type were previously undertaken by Baranyi [3, 4] employing a very precise grid-based Eulerian type method of CFD for solving the two-dimensional Navier Stokes equations. Vortex cloud modelling provides a quite different CFD method based on Lagrangian modelling of the same situation and the second aim of this paper is to compare results obtained by these two techniques of fluid-flow simulation. Such comparisons of the now well established CFD codes for classical datum cases are crucial at this stage of increasingly wide engineering design/analysis application and one such paper has already been published by Baranyi and Lewis [5] for low Re flow past a stationary cylinder. The present paper extends these cross-checks to cylinders in orbital motion.

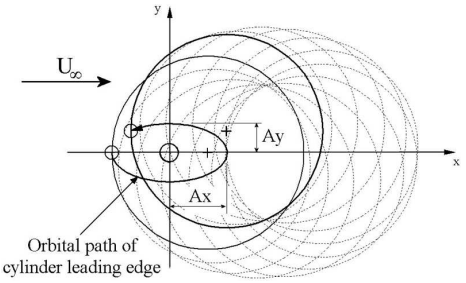

Figure 1. Elliptical path for a cylinder in orbital motion

The main advantage of the vortex cloud model is its ability to keep account of all the vorticity in the downstream wake without the restriction of any reference grid and the consequent ease for obtaining simulated wake patterns. A full account of the fundamentals of vortex cloud analysis has been given by Lewis [9] and of its application to moving bodies and cascades [10, 11]. Thus only a brief summary of the underlying theory will be given here in section (2) followed in section (3) by comparisons of predicted lift and drag coefficients and presentation of selected wake patterns. Before proceeding with this we begin with a presentation of the underlying geometrical definitions of the proposed orbital motion as illustrated in Figure 1.

As shown here the cylinder is located in a uniform stream U_∞ but subjected to an orbital motion following an elliptical path with semi-major and minor axes A_x , A_y where the cylinder leading edge point O is taken here to define this path. In practice oscillations might occur with different frequencies f_x and f_y parallel to the x and y axes. For elliptical motion however we will impose equal values $f = f_x = f_y$ and adopt anticlockwise motion beginning in the downstream direction for which the cylinder displacements at time t are given by

$$x_0 = -A_x \cos(2\pi f t), \quad x_0 = -A_y \sin(2\pi f t) \tag{1.3}$$

and its velocity components u_0 and v_0 are thus

$$u_0 = 2\pi f A_x \sin(2\pi f t), \quad v_0 = 2\pi f A_y \cos(2\pi f t). \tag{1.4}$$

2. **The vortex cloud flow simulation method**

The flow model for vortex cloud analysis is illustrated in Figure 2. At any instant the flow past the cylinder generates a surface vorticity sheet of local strength $\gamma(s) = v_s$ equal in magnitude to the surface slip-velocity v_s. If the cylinder is represented by M surface elements, the vorticity at element n is assumed to be shed as a discrete vortex element of strength $\Delta\Gamma_n = \gamma(s_n)\Delta s_n$. Although only 12 elements are shown in Figure 2, typically fifty surface elements would be adopted for acceptable resolution as in the present project. For further accuracy sub-elements may be used as illustrated in Figure 2(b), where the line vortex element $\gamma(s_n)\Delta s_n$ has been modelled by three sub-elements of strength $\Delta\Gamma_n = \frac{1}{3}\gamma(s_n)\Delta s_n$.

The governing integral equation is then given by [9]

$$\begin{aligned} &\tfrac{1}{2}\gamma(s_m) + \oint k(s_m, s_n)\,\gamma(s_n)\,ds_n + (U_\infty - u_0)\cos\beta_m + (V_\infty - v_0)\sin\beta_m + \\ &+ \sum_{j=1}^{Z} \Delta\Gamma_j \,(U_{mj}\cos\beta_m + V_{mj}\sin\beta_m) = 0 \end{aligned} \tag{2.1}$$

which states that the velocity on and parallel to the body surface of point m is zero. This equation may be represented numerically by the following set of M linear

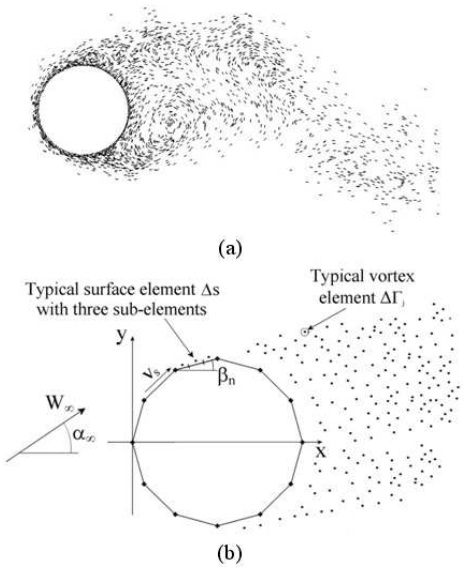

Figure 2. Numerical model for vortex cloud analysis. (a) Vortex cloud wake flow simulation, (b) Numerical model

equations,

$$\sum_{n=1}^{M} K\left(s_m, s_n\right)\gamma\left(s_n\right) = -\left(U_\infty - u_0\right)\cos\beta_m - \left(V_\infty - v_0\right)\sin\beta_m - \\ - \sum_{j=1}^{Z} \Delta\Gamma_j\left(U_{mj}\cos\beta_m + V_{mj}\sin\beta_m\right) \tag{2.2}$$

where the cylinder is located in the uniform stream W_∞ and Z discrete vortex elements $\Delta\Gamma_j$ have been shed into the fluid since initiation of the motion.

The vortex cloud computations are undertaken in a time-stepping sequence, in the present case for 3000 steps of size $\Delta t = 0.05$, with a uniform stream $W_\infty = U_\infty = 1.0$ and a cylinder diameter $d = 1.0$. A summary of the computations undertaken for each time step is as follows:

Vortex Cloud analysis time-stepping procedure

1. Potential flow analysis by equation (2.2), to calculate the body surface slip flow and the newly created surface vorticity $\gamma(s_j)$.

2. The shedding of discrete vortices $\Delta\Gamma_j = \gamma(s_j)\Delta s_j$ from each surface element, thus creating a cloud of vortex elements.

3. Use of the random walk procedure [9] for each discrete vortex $\Delta\Gamma_j$ to simulate viscous diffusion over the time step Δt.

4. Mutual convection of all members of the vortex cloud for this time step.

5. Recombination of any vortices that become excessively close due to the random walk. This has the beneficial side effect of reducing the total volume of the vortex cloud.

6. Deletion of any discrete vortices which stray inside the body profile during diffusion and imposition of the circulation theorem to ensure that the equivalent loss is restored during the subsequent potential flow analysis (Step 1 above) in order to ensure overall conservation of vorticity.

Output data of importance to categorise the resulting motions are the predicted vortex wake motions and the lift and drag coefficients C_L, C_D. In view of the oscillatory nature of the latter, helpful practice is to evaluate their average values and their rms fluctuations, defined as follows.

$$\begin{aligned} C_{Lmean} &= \frac{1}{t_2-t_1}\int_{t_1}^{t_2} C_L dt \\ C_{Lrms} &= \sqrt{\frac{1}{t_2-t_1}\int_{t_1}^{t_2} [C_L - C_{Lmean}]\, dt} \end{aligned} \tag{2.3}$$

and similarly for C_{Dmean} and C_{Drms}, where the interval t_1 to t_2 includes a large number of completed oscillations.

3. **Predicted results for three test cases**

Baranyi [3] published results predicted by his grid-based CFD method for the three configurations given in Table 1, which will be the focus of the present studies. The orbital semi-major axis A_x is fixed at 0.3 for all cases and the semi-minor axis is varied over the range $0.0 \leq A_x \leq 0.3$. For each Re value the orbital frequency f is set at 85 % of the Strouhal number for the fixed cylinder.

Table 1. Parameters for test cases

Case	Re	f	A_x	A_y range
1	130	0.1521	0.3	0.0 to 0.3
2	160	0.1598	0.3	0.0 to 0.3
3	180	0.165665	0.3	0.0 to 0.3

Vortex cloud calculations were undertaken for these three test cases for a cylinder modelled by 50 elements, with two sub-elements. Further to this, to reduce the "numerical noise" inherent in the random walk model for viscous diffusion, it was also decided to undertake the viscous diffusion in three sub-steps of value $\frac{1}{3}\Delta t$. Vortex cloud predictions will now be presented for these three cases in comparison with Baranyi [3].

3.1. **Case 1:** Re = 130**,** $f = 0.1521$**.** The mean and rms lift and drag coefficients are compared in Figure 3, where, of particular interest, are the predicted C_{Lmean} values. As previously predicted by Baranyi, Figure 3(a), these resolve into two distinct envelopes that show a major discontinuity in the lower range of A_y values. His results shift discontinuously from the upper envelope to the lower one at $A_y \approx 0.02$ and revert to the upper at $A_y \approx 0.07$.

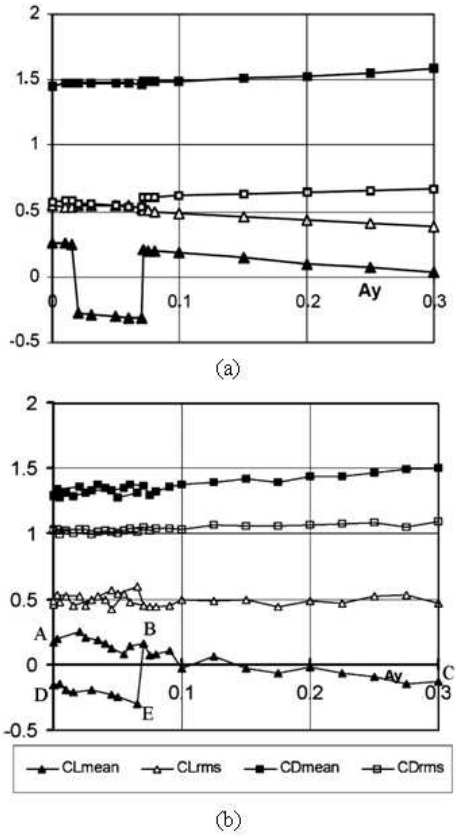

Figure 3. Comparison of predicted force coefficients for Re = 130,f = 0.1521, $A_x = 0.3$. (a) Baranyi [3] – Grid based method, (b) Lewis – Vortex cloud method

The present vortex dynamics predictions, Figure 3(b), show good general agreement of C_{Lmean} with Baranyi's results but with some very interesting variations in the lower range $A_y < 0.07$ for which results fell on either the upper envelope ABC or the lower one DEB. The immediate deduction to be drawn from this is the likelihood of some major instability between two possible stable vortex wake regimes and we will return to this later. Good agreement was also obtained between the two methods for the

predicted values of C_{Lrms} and C_{Lmean} but less so for C_{Lrms} for which vortex cloud modelling shows much higher values.

Next we will take a look at the actual variations of C_L and C_D with time, see Figure 4 below.

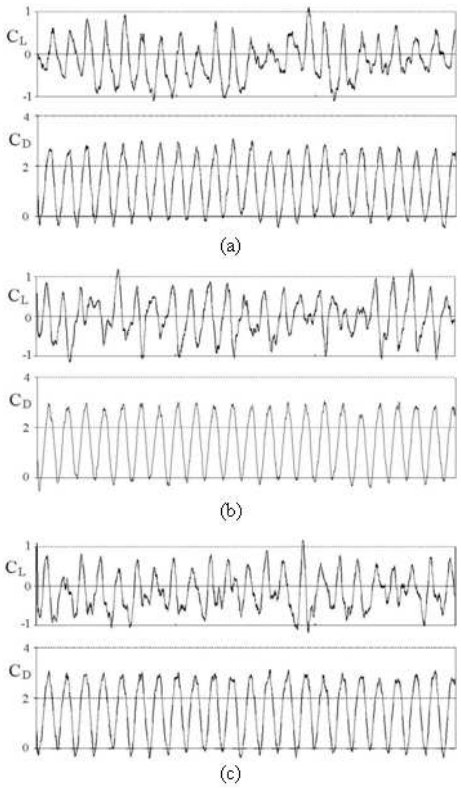

Figure 4. Predicted lift and drag coefficients for Re = 130, f = 0.1521. (a) $A_x = 0.3$, $A_y = 0.0$, (b) $A_x = 0.3$, $A_y = 0.15$, (c) $A_x = 0.3$, $A_y = 0.3$

The predicted variations with time of C_L and C_D are shown in Figure 4 for $A_x = 0.3$ for three values of A_y spanning the orbital range from purely horizontal motion $A_y = 0.0$, on to elliptical motion $A_y = 0.15$ and finally for circular motion $A_y = 0.3$. The C_D curves are remarkably similar which explains the fairly constant values for C_{Dmean} and C_{Drms} in Figure 3 and it is of some interest to note that this wide variation in orbital motion should have such little impact on the magnitude and character of the drag coefficient. On the other hand much more variation can be observed in the predicted lift coefficient C_L. There are fluctuations in the amplitude and variations in the predicted wave pattern for all three cases but increasingly so as the vertical

orbital displacement Ay is increased. The most regular of these is for horizontal motion $A_y = 0.0$, Figure 4(a), particularly over the first half of the time sequence. Attention should be drawn to the general wave shape which has sharp maxima and more rounded minima, a characteristic discovered by Baranyi [3]. This same feature is conspicuous in Figure 4(c) for circular motion, $A_y = 0.3$, if less conspicuously so for the elliptical orbit, Figure 4(b).

For further insight into some of these characteristics we will now focus attention on predicted wake patterns for these three orbital cases, Figure 5.

Figure 5 portrays the predicted wake patterns for these three cases in comparison with that for the motionless cylinder with its typical von Kármán vortex street, Figure 5(a). Here the cylinder in practice sheds vortices of alternate sign and equal magnitude into the wake at regular intervals, namely the Strouhal frequency St, as borne out here by vortex cloud simulation. The predicted flow pattern for purely horizontal motion, Figure 5(b), is quite similar to this but with some evidence of vortex pairing of the two +ve and −ve vortices shed during each orbit. For the cylinder in orbital motion however, Figures 5(c) and 5(d), much more development of this phenomenon is observed, namely the formation in the wake of very distinct vortex pairs. Thus in Figure 5(c), attention is drawn to the pairing of a clockwise +ve vortex shed from the upper surface with an anticlockwise −ve vortex shed slightly previously from the lower surface and we observe also a new vortex pair being shed just downstream of the cylinder as it completes it's upstream orbiting motion. These +/− vortex pairs have a natural self-convection effect in the downwards direction resulting in a general net downward drift of the cylinder wake. The same phenomenon can be observed in Figure 5(d) for the circular orbit. Once again the vortex pairing is of +/− type as for the elliptical orbit, Figure 5(c). It is of particular interest to observe however that the opposite +/− vortex pairing occurred for the case of purely horizontal motion $A_y = 0.0$ shown here in Figure 5(b). In this case, Figure 3(b), the related C_{Lmean} value was at point D located on the lower envelope whereas the C_{Lmean} values for the elliptical and circular orbiting cases $A_y = 0.15$ and 0.3 actually lie on the upper envelope. There thus seems to be a direct connection between the sign of vortex pairing and the particular envelope on which the C_{Lmean} results lie.

3.2. **Case 2:** Re = 160**,** $f = 0.1598$**.** Results for the higher Reynolds number of Re = 160 are shown in Figure 6 where the behavioural trends of C_{Lmean} are again similar for the two CFD methods, with good agreement for the wider orbiting range $0.15 < A_y < 0.3$. As before Baranyi discovered the switching of C_{Lmean} between upper and lower envelopes, in this case for $A_y > 0.07$. However it is of considerable interest to note that his predicted C_{Lmean} curve is an inversion of that for Re = 130, Figure 5(a). Vortex cloud predictions here suggest a more progressive switch over the range $0.09 < A_y < 0.15$ and many more points were obtained on the lower envelope than the upper for $A_y < 0.08$. The reason for the greater stability of the C_{Lmean} curves for the higher A_y values is probably due to the stronger stirring effect of the wider elliptical orbit shedding large amounts of clockwise vorticity. This leads here

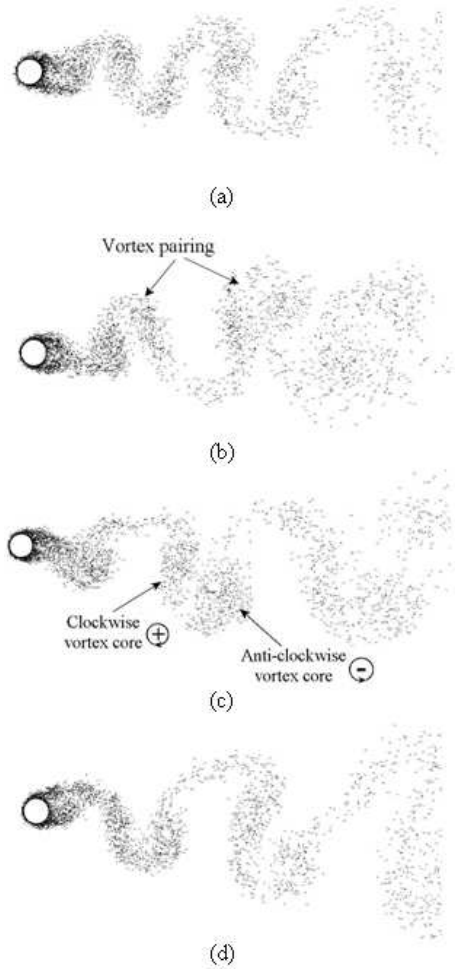

Figure 5. Predicted wake flow for Re = 130 for various orbits. (a) Motionless cylinder with zero orbital motion, $f = A_x = A_y = 0.0$, (b) Cylinder in orbital (horizontal) motion with $f = 0.1521$, $A_x = 0.3$, $A_y = 0.0$, (c) Cylinder in orbital (elliptical) motion with $f = 0.1521$, $A_x = 0.3$, $A_y = 0.15$, (d) Cylinder in orbital (circular) motion with $f = 0.1521$, $A_x = 0.3$, $A_y = 0.3$

to anticlockwise bound vorticity and large negative lift. However, one stray point A was found for $A_y = 0.21$ seeming to lie on the extended upper envelope, Figure 6(b).

A re-run of this situation resulted in the C_{Lmean} value B lying on the lower envelope having the normal vortex pairing, as can be seen from Figure 7 below.

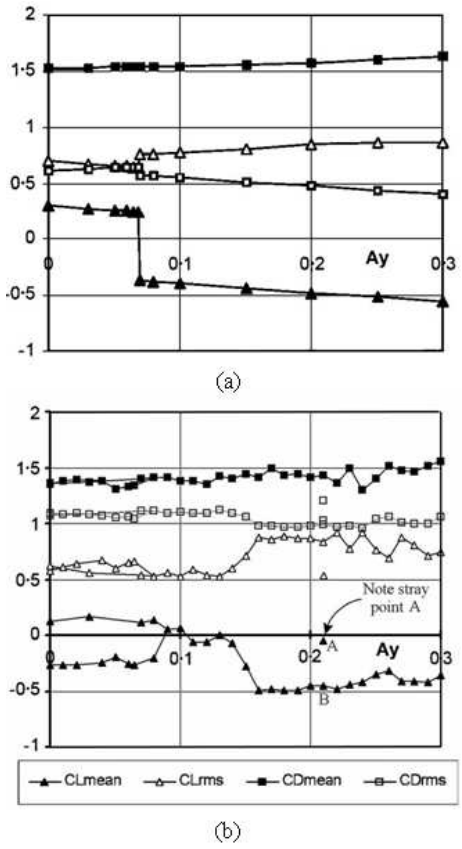

Figure 6. Comparison of predicted force coefficients for Re = 160, $f_x = f_y = 0.1598$, $A_x = 0.3$. (a) Baranyi – Grid based method, (b) Lewis – Vortex cloud method

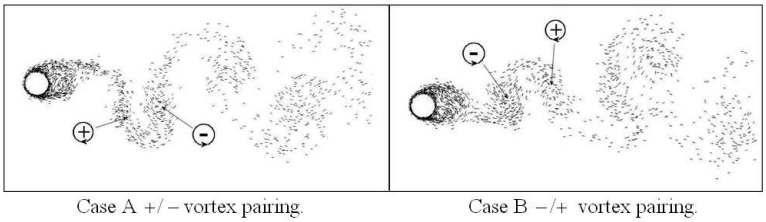

Figure 7. Opposite vortex pairing of points A and B in Figure 6

As can be seen from Figure 7, the stray point A has $+/-$ vortex pairing which is opposite to the normal more stable $-/+$ pairing of Case B. What is of particular

importance to note here however is that at the higher Re of 160 the vortex pairing for the wider y orbital range of $0.07 < A_y < 0.3$ of stable vortex motion is of Case B $-/+$ type which is quite contrary to that exhibited for Re = 130 orbital motion where the stable vortex pairings were of $+/-$ type, a remarkable switch of behaviour for such a small Reynolds number rise. Comparing Baranyi's results for these two Reynolds numbers, Figures 5(a) and 6(a), the same shift of vortex pairing between the $+/-$ and $-/+$ types was in all probability also occurring, judging by the shift from the upper envelope to the lower for $A_y > 0.07$. We now consider results for a further increase to Re = 180 for the same orbital motions.

3.3. **Case 3:** Re = 180**,** $f = 0.165665$**.** Predicted results for the third case at the highest Reynolds number Re = 180 with orbital frequency $f = 0.165665$ are shown in Figure 8. As before Baranyi [3], Figure 8a, found there to be two envelopes, with a fairly similar distribution of C_{Lmean}. Thus all C_{Lmean} values for $A_y > 0.1$ are lying on the lower envelope following the same trend as the Re = 160 results. For $A_y < 0.l$ on the other hand his predicted values lay mainly on the upper envelope with deviations from this in the very low y amplitude range $A_y \approx 0.004$ to 0.02.

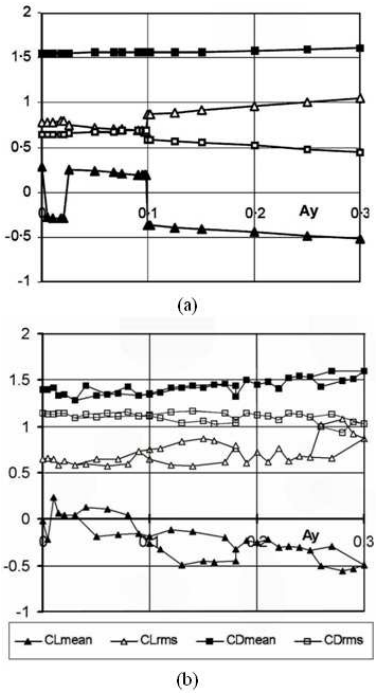

Figure 8. Comparison of predicted force coefficients for Re = 180, $f_x = f_y = 0.165665$, $A_x = 0.3$. (a) Baranyi – Grid based method, (b) Lewis – Vortex cloud method

Vortex cloud analysis predicted similar overall trends for the lower envelope for $A_y > 0.1$ but also, surprisingly, the presence of an upper envelope over most of this wider orbiting range. The strategy adopted here on the evidence of Section 3.2 was to plot points with $+/-$ vortex pairing on the upper envelope and $-/+$ pairs on the lower one. Within the small range $0.18 < A_y < 0.25$, however, no points were found on the lower envelope. It is difficult to escape the conclusion, comparing Figures 3, 6 and 8, that these developments of the upper envelope for the range $A_y > 0.1$ at the increasing Reynolds number are caused by the progressive dominance of convection over viscous diffusion. At the lower orbital range of $A_y < 0.1$ the same indeterminacy of vortex pairing type is present and the upper envelope is in good agreement between the two CFD methods. A couple of points were, however, still found on the lower envelope by vortex cloud modelling.

Another feature of test runs for Re = 180 was the tendency so switch occasionally between the $+/-$ and $-/+$ vortex pairing modes for some of the A_y values. Similar switching occurred to a very limited extent at Re = 160 in the lower A_y range. At these lower Re values of 130 and 160 however stable locking of the vortex pairs generally occurred as the norm for each test run.

4. **Conclusions**

The following conclusions may be drawn from this study:

1. Reasonable agreement has been obtained between a high resolution grid based CFD method and vortex cloud modelling of cylinders in orbital motion within the low Re range 130 to 180, with special focus on the time averaged lift coefficient C_{Lmean}. Best agreement was obtained at the lower Reynolds number Re = 130.
2. Although vortex shedding is dependent ultimately upon boundary layer formation and separation, which is more rigorously modelled in the grid-based method of Baranyi, for bluff body flows periodic vortex shedding is also strongly dominated by the upstream influence of vortex formation and convective patterns within the downstream wake for which both CFD methods are well adapted.
3. Both methods revealed the presence of upper and lower envelopes of the C_{Lmean} curves. For Re = 130 results for the larger y orbits over the range $0.1 < A_y < 0.3$ lay on the upper envelope. For Re = 160 and 180 however C_{Lmean} values predicted by Baranyi lay on the lower envelope over this range.
4. For the higher Reynolds number Re = 180, however, the present method predicted the presence of C_{Lmean} values lying on both upper and lower envelopes over almost the entire y orbiting range $0.023 < A_y < 0.3$ which has been attributed to the greater influence of convective motions as one approaches the upper limit of Re $\approx$ 190 below which the flow locks into two-dimensional motion and above which three-dimensional instabilities begin to set in.
5. The present studies have revealed that the orbital motion results in regular vortex pairing in the downstream wake. These are shown to be of the two

possible types, namely +/− and −/+.Points on the upper envelope are found to be of +/− type and those on the lower envelope are of −/+ type.

6. Wake patterns at the higher Re = 180 were sometimes found to switch between +/− and −/+ type, whereas at the lower Reynolds numbers much more stable locking of the vortex pairs was occurring as the norm.

REFERENCES

1. Strouhal, V.: Über eine besondere Art der Tonerregung. *Ann. Phys. und Chemie. Nav. Series* **5**, (1878), 216-251.
2. Kármán T. von.: Über ein Mechanismus des Widerstandes, den ein bewegter Körper in einer Flüssigkeit erfährt. *Göttingen Nachrichten Maths, -Phys.*, (1911), KI., 509-517.
3. Baranyi, L.: Numerical simulation of flow past a cylinder in orbital motion. *Journal of Computational and Applied Mechanics* **5**(2), (2004), 209-222.
4. Baranyi, L.: Lift and drag evaluation in translating and rotating non-inertial systems. *Journal of Fluids and Structures*, **20**, (2005), 25-34.
5. Baranyi, L. and Lewis, R.I.: Comparison of a grid-based CFD method and vortex dynamics predictions of low Reynolds number cylinder flows. *The Aeronautical Journal*, **110**(1103), (2006), 63-71.
6. Barkley, D. and Henderson, R.D.: Three-dimensional Floquet stability analysis of the wake of a circular cylinder. *Journal of Fluid Mechanics*, **332**, (1996), 215-241.
7. Posdziech, O. and Grundmann, R.: Numerical simulation of the flow around an infinitely long circular cylinder in the transition regime. *Theoretical and Computational Fluid Dynamics*, **15**, (2001), 121-141.
8. Williamson, C.H.K.: Vortex dynamics in the cylinder wake. *Annual Review of Fluid Mechanics*, **28**, (1996), 477-539.
9. Lewis, R.I.: *Vortex Element Methods for Fluid Dynamic Analysis of Engineering Systems*. Cambridge University Press, Cambridge, 1991.
10. SLewis, R.I.: Development of Vortex Dynamics for Simulation of Turbomachine Cascades and Blade Rows. *J. Comp. App. Mech.*, **2**(1), (2001),73-85.
11. Lewis, R.I.: Study of blade to blade flows and circumferential stall propagation in radial diffusers and radial fans by vortex cloud analysis. *Journal of Computational and Applied Mechanics*, **5**(2), (2004), 323-335.